Received: 25 November 2022 | Revised: 9 February 2023 | Accepted: 24 February 2023

IET Renewable Power Generation

DOI: 10.1049/rpg2.12711

The Institution of Engineering and Technology WILEY

ORIGINAL RESEARCH

# Demystifying inertial specifications; supporting the inclusion of grid-followers

**Sam Harrison** | **Callum Henderson** | **Panagiotis N. Papadopoulos** | **Agusti Egea-Alvarez**

Department of Electronic and Electrical Engineering, University of Strathclyde, Glasgow, UK

**Correspondence**
Department of Electronic and Electrical Engineering, University of Strathclyde, Glasgow, UK.
Email: sam.harrison@strath.ac.uk

**Abstract**

Inertial response from grid-followers (GFLs) is deemed to be "synthetic" due to a slow response. In contrast, grid-forming (GFM) inertial response is deemed to be faster and therefore "true" and more useful for frequency stability. This paper explores the differences and similarities between an established example of a GFM and a GFL inertial controller by carrying out parametric sweeps at different operating conditions. The analysis aims to assist the ongoing efforts to quantify grid stabilising phenomena, particularly the recent adaptation of the British grid code to incorporate GFM converters. The optimal tuning configurations are identified, showing that some configurations of the GFL can achieve fast inertial provision on strong grids. These configurations are shown to contain the grid frequency as effectively as the GFM, despite the opposing consensus in the literature. The results also highlight the importance of voltage-source behaviours in determining the initial evolution of grid frequency. Although a blanket inclusion of all GFL inertial configurations is not appropriate, equally, the existing blanket disqualification could limit the assets available to support GFMs (who will certainly be required to stabilise the grid in a fundamental sense) and could inhibit the rate that the net zero transition can occur.

## 1 | INTRODUCTION

The dynamic behaviour of a synchronous machine (SM) provides many features that stabilise the electrical grid. Their voltage-source behaviour establishes the system voltage angle (and hence frequency) and provides transient power injections that contain its variation following disturbances. Their inertial energy storage acts as a physically coupled reserve that can resolve power imbalances quickly and hence limit the system's rate of change of frequency (ROCOF). Both features are inherent to SMs and are critical to system stability [1]. However, articular focus has been made on the link between inertial energy storage and the risk of large ROCOFs [2] as the penetration of converter interfaced devices increases on systems such as Great Britain, Ireland, and Australia [3]–[5].

Grid-forming (GFM) controllers were developed to enable converters to provide the system stabilising features that SMs had previously provided inherently. Controllers were developed to emulate the Swing Equation, which describes the SM's inertial power injection [1], alongside other SM dynamic equations. As a result, GFMs are operated as voltage-sources [6]. As the initial approaches emulated the SM's Swing Equation, many were fundamentally linked to inertial dynamics, for example, the family of Virtual Synchronous Machine (VSM) controllers [7], [8]. However, other implementations did not include inherent inertial dynamics, such as the first order GFM Droop controller, which instead emulates the power-frequency droop relationship that governs SM power balancing [9]. This approach does, however, continue to operate as a voltage-source.

Additional GFM control concepts continue to be proposed, some which inherently possess inertial behaviour, for example, matching control [10], and others which do not, for example, virtual oscillator control [11]. Adapted configurations of the initial GFM controllers have also been developed that can: decouple their inertial and droop responses to achieve improved damping [12], decouple the active and reactive channels to minimise undesired transient variations [13], utilise a current-control framework to achieve improved small-signal stability

across a range of short circuit ratios (SCRs) (also linked to the power coupling issue) [14], or implement adaptive inertia settings to achieve optimal operation depending on the system conditions [15]. However, none of the simple or advanced control configurations change the fundamental features of the inertial response (IR).

The conventional converter control strategy, Current Control (CC), is described as grid-following (GFL) due to its objective to synchronise with the grid's voltage angle. This fundamental difference in operating principle is the reason that GFMs have been the focus of such research interest recently, as they hold the key to establishing a grid voltage without SMs. CCs also experience issues in weak grids, where their outer loops can be destabilised at high power levels due to a coupling between the active and reactive power controllers [16]. Despite these features, CC is an established technology that is widely implemented and solutions exist to overcome their instability in weak grids [16]. Although CC does not inherently provide IR, it can be adapted to do so [17], enabling a larger fraction of the converter capacity to support grid stability (and remove the strain on GFMs who will be required to provide many other stabilising features) while maintaining the useful benefits of CC: the effective limitation of the current.

GFL inertial controllers are not commonly implemented due to the conventional assumption that their response is delivered too slowly to be useful. [18] showed that an averaging window configuration for the GFL's ROCOF measurement constrained the IR speed and significantly reduced its ability to support the grid's frequency compared to a GFM. However, this assessment only considered one specific ROCOF measurement approach. Similarly, other comparisons that found GFM IR to stabilise power system frequency better only considered a single GFL control tuning configuration [19], [20], despite other studies that show the tuning to have a large impact on GFL inertial dynamics [21] and a range of tunings being experimentally validated [22].

The former studies [18]–[20] have resulted in the labelling of GFM inertial controllers as possessing "true" and useful inertial capability and of GFL inertial controllers as having "synthetic" and less (or not) useful inertial capability [23]–[27]. Confusingly, synthetic inertia is a term that has also been used to describe fast-frequency droop-type active-power responses to frequency deviations, but this terminology has been shown to be incorrect [28].

The assumption of slow GFL IR may also be linked to the confusion of inertial and voltage source dynamics. The recent development of industrial inertial specifications exhibits this link; the thresholds that are used to disqualify GFL IR often resemble voltage-source transient phase response timescales [9], [10], [11]. Great Britain's System Operator (SO), National Grid Electricity System Operator (NG ESO), definition of the minimum non-mandatory characteristics for GFMs (that may form the basis of a future stability market) [9] and the definition of "true" inertial capability according to the collection of European SOs [26] require converters to be able to provide IR without frequency measurement and for the response to initiate instantly (where instant is equated to a 5 ms delay). The Australian Electricity Market Operator's definition of "true" IR corresponds to a full response delivery within the effectively instant 5 ms timeframe [24]. In reality, unlike ideal transient voltage-source injections, IR is not delivered instantly [19] so the GFL's frequency measurement may not be as significant as previously thought.

**TABLE 1** Table of abbreviations.

| | | | |
|---|---|---|---|
| AC | Alternating current | PCC | Point of common coupling |
| CC | Current control | PI | Proportional-integral |
| DC | Direct current | PLL | Phase locked loop |
| dq | Direct-quadrature | ROCOF | Rate of change of frequency |
| EMT | Electro-magnetic transient | RT | Rise time |
| GFL | Grid-following | SCR | Short circuit ratio |
| GFM | Grid-forming | SM | Synchronous machine |
| LCL | Inductor-capacitor-inductor | SO | System operator |
| NFP | Network frequency perturbation | ST | Settling time |
| NG ESO | National Grid Electricity System Operator | VSM | Virtual synchronous machine |
| OS | Overshoot | | |

This paper provides several contributions:

1. An explicit outline of the differences between inertial and transient phase responses and their impact on system frequency.
2. A conclusive assessment if useful IR can only be sourced from GFMs.
3. An assessment of the ability of the industrial specifications to identify the useful features of IR.

The differences between IR and transient response are defined in Section 2. Section 3 details the example GFM and GFL converters and the grid systems that will be assessed throughout the paper. Section 4 describes the methodology, which includes parametric sweeps of the example controllers to assess how their inertial properties change and the use of a multi-bus power system to explore the properties further. Section 5 reviews the methods available to identify useful IR and outlines the criteria that is used for its qualification. Section 6 presents the results: substantiating the differences between IR and transient phase response defined in Section 2, assessing if the GFL IR can ever meet the useful IR criteria, and assessing the impact that features of the different controllers' responses have on the system frequency. All of the abbreviations used throughout the text are detailed in Table 1.

These results will inform the development of specifications for useful frequency-stabilising services and can either enable the assertion to continue to focus only on GFM iner-

tial solutions, or, can offer a wider range of potential solutions to support GFMs increasing system inertia. The results of this paper do not aim to provide a single conclusive optimal approach to provide IR, but rather, to discuss the existing misconception that useful IR is unique to GFMs.

## 2 | THEORETICAL DEFINITIONS OF INERTIAL AND VOLTAGE-SOURCE BEHAVIOUR

Conventionally, the grid has been stabilised by SMs, which possess both inertial and voltage-source properties. Although distinct, the two stabilising features appear to have been confused in recent GFM specifications, potentially due to the inherent provision of both features on conventionally SM dominated systems.

GFMs operating in the linear area (and SMs) are operated as voltage sources; they establish a constant internal voltage that connects to the grid via a series impedance [29]. The voltage-source operation allows the GFM to respond inherently to transient disturbances on the grid. This behaviour can be visualised by (1), which describes the power flow $P$ between two voltage sources with a coupling impedance $X_L$, and is an accurate representation of a GFM delivering power to the grid.

$$P = \frac{V_c V_g}{X_L} \sin(\delta), \tag{1}$$

where $V_c$ and $V_g$ are the sending and receiving voltage sources' magnitudes and $\delta$ is the angular difference between the sending $\theta$ and receiving $\phi$ voltage sources' angles. If the GFM's voltage magnitude $V_c$ and angle $\theta$ are constant, a change in any of the grid's properties will result in an immediate change in the power that is injected to the grid. For example, if a step in the load increases the angular difference between the GFM and the grid more current and power will immediately be drawn from the GFM (described as the transient phase response). This response is equivalent to the action of synchronising torque between SMs, which is described as the rate of change of power with respect to angle that maintains their synchronism and contributes to transient system stability [1].

In contrast, inertial behaviour is expressed by the swing Equation (2), which describes the link between a SM's mechanical system and its electrical stator (i.e. coupled with the grid dynamics).

$$\frac{d^2\theta}{dt^2} = \frac{\omega_0}{2H}\left(P_m - P - K_d\Delta\omega\right), \tag{2}$$

$\omega_0$ is the synchronous speed, $H$ is the inertia constant of the SM, $P_m$ is the mechanical power being input to the SM, $K_d$ is the SM's damping coefficient and $\Delta\omega$ is the difference between the SM's electrical frequency $\omega$ and $\omega_0$. This electromechanical equation describes the balance of mechanical power input and the electrical power extracted from the spinning SM, whose stored kinetic energy balances any mismatches between the two via changes in rotational speed. Equation (22) does not describe a behaviour that is unique to an electrical voltage source. (2) can be used to describe an inertial device's power response to a grid frequency disturbance. This equation is used in the industrial inertial specifications [9], [10], [11] to quantify a device's contribution to grid frequency stability in terms of a response to a ROCOF.

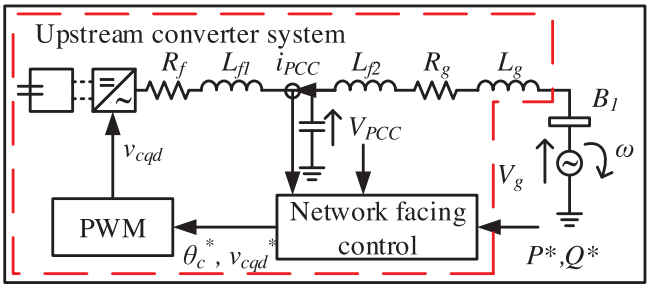


**FIGURE 1** Electrical diagram of converter model with ideal DC energy source connected to infinite bus representation of grid, via LCL filter

A voltage-source's transient phase response (1) can impact its inertial behaviour (2) but the two are distinct. (11) describes the instantaneous behaviour that determines an initial angular acceleration [30] that would then drive an IR. However, if a non-inertial voltage source (such as the first order droop [9] or the VSM0H [18] controller) was subject to the same disturbance, (1) would continue to determine the initial angular change but would not result in any second order inertial behaviour.

## 3 | SYSTEM UNDER STUDY

A model of an ideal battery connected to a power network via a converter is built to compare the IR from an example of a GFM (Proportional-integral (PI) VSM) and a GFL (CC) controller. An ideal energy source is utilised as the comparison is interested in the differences between the two controllers (both of which would be affected by specific energy source dynamics such as those exhibited for wind turbines in [31]). The control configurations assessed in this study are selected to resemble the GFM strategy detailed in the NG ESO industrial specification [23] and the standard industrial GFL inertial strategy. Moreover, they achieve similar fundamental inertial delivery properties as advanced strategies [12]–[15] so provide an effective baseline to assess the ability of an example of a GFM and a GFL to meet the industrial criteria for useful IR, beyond which both approaches could be developed and improved upon in the future.

The model is composed of an average representation of a voltage-source converter with the ideal battery energy source on the DC-side. The converter is connected on the AC-side via an LCL filter to a Thevenin Equivalent representation of the grid (Figure 1). The model represents the grid as an infinite bus, which imposes a grid frequency change on the converter. By doing so, the converter's exact IR to an ideal frequency change (ROCOF) can be observed without any overlap with the GFM's inherent voltage-source response features (e.g. transient phase

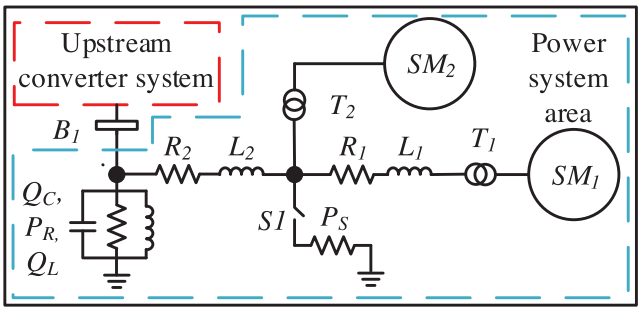


**FIGURE 2** Electrical diagram of the power system model area that is connected via bus B1 to the upstream components of the converter system pictured in Figure 1

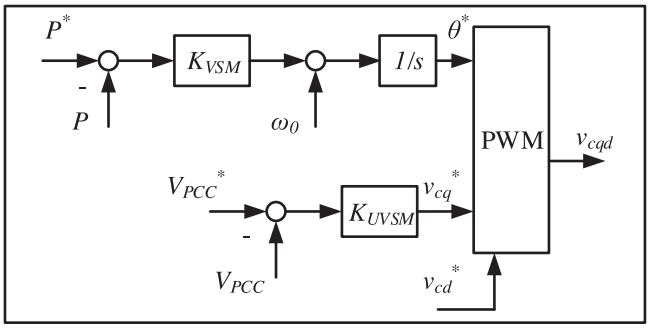


**FIGURE 3** GFM control strategy boxplot

response). The grid strength can be represented by the SCR, which determines the grid resistance $R_g$ and inductance $L_g$ that the converter connects to.

Parametric sweeps of the control and network configurations are carried out to assess the capability of the different controllers using small-signal models, the full derivation of which can be found in [32]. The small-signal models are validated by comparing their active power response to a frequency disturbance input with that of an equivalent electro-magnetic transient (EMT) time-domain model. The GFM small-signal model achieves a steady-state error of −3.9% while the GFL achieves a steady-state error of −0.38% compared to their respective equivalent EMT models (.

Another EMT time-domain model (pictured in Figure 2) is built to assess the impact that the different control configurations have on system frequency. The model is developed from the Matlab power_PSS example, which is detailed in [33] and is itself based on Kundur's two area system model [1]. The main adaptations made to the Matlab example are: 1) the replacement of any components upstream of bus $B_1$ with a single aggregated converter station that is topologically identical to the components within the red box on the infinite bus system in Figures 1 and 2) the reduction of the SM inertia constants to $H = 2$ s, and 3) the addition of an active load behind a switch ( $P_s = 10$ MW) to simulate a grid disturbance and IR. The remaining system parameters are detailed in the Appendix and the base control configurations are shown in Table 2, which were tuned to be able to provide a stable IR and an acceptable settling time in response to active power and voltage reference steps across the range of tested conditions for a standard inertial value.

## 3.1 | Grid-forming control

The GFM control strategy (pictured in Figure 3) is based on a VSM with two PI controllers, one for the power and another for the voltage control actions [32], [34]. The power controller $K_{VSM}$ uses its proportional $K_{p,VSM}$ and integral $K_{i,VSM}$ gains to act on the error of the converter power $P$ with respect to its reference $P^*$ and sets the converter's internal angle reference $\theta^*$, as shown in (3).

$$\theta^* = \frac{K_{VSM}\,(P^* - P) + \omega_0}{s}. \tag{3}$$

The converter voltage magnitude $V_c$ is then formed in the dq frame, where the d component is set to zero (4) and the q component is determined according to the action of the voltage controller's $K_{UVSM}$ proportional $K_{p,UVSM}$ and integral $K_{i,UVSM}$ gains on the error between the point of common coupling (PCC) voltage $V_{PCC}$ and its reference $V_{PCC}^*$ (5).

$$v_{cd}^* = 0, \tag{4}$$

$$v_{cq}^* = K_{UVSM}\,\left(V_{PCC}^* - V_{PCC}\right). \tag{5}$$

**TABLE 2** Base control parameters.

| | | | | | |
|---|---|---|---|---|---|
| **GFM** | | | | | |
| $H$ | Inertial constant | 2 (s) | $\zeta_{VSM}$ | Damping coefficient | 0.42 |
| $K_{pUVSM}$ | Voltage proportional gain | $1 \times 10^{-2}$ | $K_{iUVSM}$ | Voltage integral gain | 239 |
| **GFL** | | | | | |
| $H$ | Inertial constant | 2 (s) | $D$ | Derivative gain | 1 |
| $\tau_{iner} = \frac{1}{\omega_{iner}}$ | Inertial-filter time-constant | 0.155 (s) | $\tau_{CC}$ | Current control time-constant | $1 \times 10^{-3}$ (s) |
| $K_{pPLL}$ | PLL proportional gain | $7.89 \times 10^{-2}$ | $K_{iPLL}$ | PLL integral gain | 1.75 |
| $K_{pP}$ | Power proportional gain | $2.9 \times 10^{-3}$ | $K_{iP}$ | Power integral gain | 1 |
| $K_{pU}$ | Voltage proportional gain | 3 | $K_{iU}$ | Voltage integral gain | 200 |

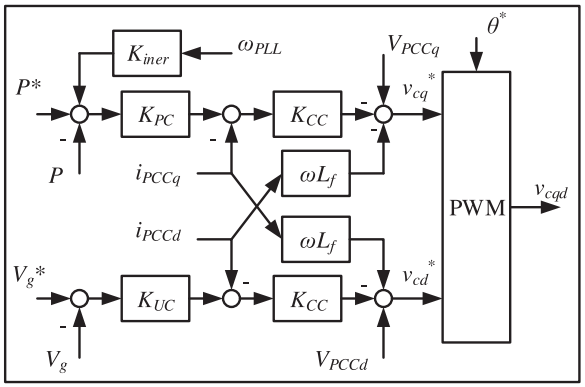


**FIGURE 4** GFL control strategy boxplot

The GFM feeds its voltage magnitude and angle components directly to the waveform modulation where the converter forms the voltage signal.

The controller's inertial capability is defined by the power controller $K_{VSM}$, which emulates the swing equation. A given inertial constant $H$ can be achieved by relating the parameters in the control transfer function (from grid frequency to converter power) to that of the swing equation, as detailed in (6) and (7).

$$K_{i,VSM} = \frac{\omega_0}{2HS_n}, \tag{6}$$

$$K_{p,VSM} = 2\zeta_{VSM}\sqrt{\frac{K_{i,VSM}}{K_s}}, \tag{7}$$

where $K_{i,VSM}$ and $K_{p,VSM}$ are the integral and proportional gains of the controller, $S_n$ is the rated power of the converter, $\zeta_{VSM}$ is the damping coefficient, and $K_s$ is the synchronising torque coefficient.

## 3.2 | Grid-following control

The GFL control strategy (Figure 4) is a standard CC with an additional inertial channel, as proposed in [17]. The inertial channel feeds the frequency measurement $\omega_{PLL}$ from the phase-locked loop (PLL) (not pictured but detailed in [35]) through a derivative block to estimate the grid ROCOF. A filter is used, with time-constant $\tau_{iner}$, to suppress noise from the derivative gain $D$. This calculation of the ROCOF is a critical difference from the averaging-window measurement used in [18], which resulted in the significant delay in GFL inertial delivery and may have driven the disqualification of GFL IRs. The derivative is then multiplied by inertial gain $K_{p,iner}$ to set the magnitude of the IR (8). This gain can be tuned by equating to the expected power response from a SM with equivalent inertia constant (9).

$$K_{iner} = K_{p,iner} * \frac{Ds}{\tau_{iner}s + 1}, \tag{8}$$

$$K_{iner} = K_{p,iner} * \frac{Ds}{\tau_{iner}s + 1}. \tag{9}$$

Intermediate-level control parameters include proportional and integral gains for the PLL ($K_{p,PLL}$ and $K_{i,PLL}$), ower controller $K_{PC}$ ($K_{p,P}$ and $K_{i,P}$), and voltage controller $K_{UC}$ ($K_{p,U}$ and $K_{i,U}$). The current controller $K_{CC}$ is the fastest control component and feeds the final voltage references to the waveform modulation. Standard rules [36] can be used to tune the controller $K_{CC}$ to achieve a given response time $\tau_{CC}$.

# 4 | METHODOLOGY

GFM specifications from industry (particularly NG ESO's [23]) and academia are reviewed in Section 5 to identify the criteria that are being used to qualify useful inertial response. Parametric sweeps of GFM and GFL controllers are then carried out at different operating points to assess how the converters' inertial delivery varies. The ability of the GFM and GFL IRs to meet the criteria will be assessed. All of the sweeps are repeated for different voltage ($V_g$ = [0.9, 1, 1.1] $PU$), power ($P$ = [0.1, 0.5, 0.9] $PU$), and SCR ($SCR$ = [1.5, 3, 5]) conditions. Finally, the optimal configurations of each controller are derived (according to the critical features of the industrial IR criteria) and are implemented on the adapted two area power system model in response to a load disturbance. The results are used to validate the stability of the controllers and to assess if either optimally tuned controller possess any inherently different properties that impact the power system's frequency.

## 4.1 | Parallel control sweep

Sweeps of the parallel control parameters that do not explicitly impact the magnitude of the IR are carried out to assess their impact on the controllers' stability and dynamics. The GFM's parallel control parameters are: $K_{p,UVSM}$, $K_{i,UVSM}$, and $\zeta_{VSM}$ (which sets $K_{p,VSM}$). The parallel control parameters assessed for the GFL are: $\tau_{iner}$ (which is represented by its inverse $\omega_{iner}$), $K_{p,PLL}$, $K_{i,PLL}$, $K_{p,PC}$, $K_{i,PC}$, $K_{p,UC}$, and $K_{i,UC}$. The GFL's CC gains are not varied as they have previously been shown to have minimal impact on the IR [37]. Each parallel-control parameter (excluding $\zeta_{VSM}$) is increased from two orders of magnitude below the base setting in Table 2 until the controller becomes unstable, while the remaining parameters are kept constant. $\zeta_{VSM}$ is varied between 0.155 and 1, spanning the range of acceptable settings described in [23]. Table 2 includes a list of the control parameters and the labels they are represented by.

## 4.2 | Inertial constant sweep

The impact that the inertial constant setting has on the controllers' stability and dynamics is also assessed to highlight: (1) the ability of each controller to support different inertia constants and (2) the impact of the inertial constant on the

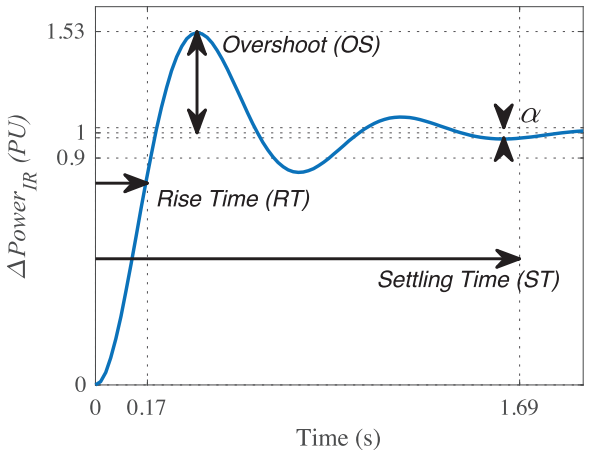


**FIGURE 5** Critical time-domain properties and corresponding values to meet the acceptable inertial criteria for an inertial response power injection $\Delta Power_{IR}$ during a frequency ramp. The power injection is normalised to the expected inertial response

IR dynamics and hence the weakness in the existing industrial approach to qualify IR by these variable features. Each controller's inertial constant is varied from $H = 0.5$ s to 6 s while the remaining parameters are tuned with a low-burden but acceptable configuration (according to the industrial criteria identified in the review) using the results of the parallel-control sweep.

## 5 | INERTIAL RESPONSE SPECIFICATION

A review of the existing methods to qualify useful IR that have been proposed in the literature [18], [19], [27] and are used in industrial specifications [23]–[25] is carried out. The methods generally use time-domain properties of the active-power inertial response, which are detailed in Section 5.1. A frequency-domain tool is also utilised in some cases, which is discussed in Section 5.2. This paper aims to assess the ability of the two controllers to meet these criteria (using the parametric sweeps on the infinite bus) as well as the ability of the criteria to identify useful IR (using the results of the power system simulations).

### 5.1 | Time-domain criteria for acceptable inertial response

Response speed is viewed as a key feature of IR in the industrial specifications [23]–[25]. GFMs delivering a large proportion of the IR before the nadir were linked to the better containment of a grid's ROCOF in [19]. To incorporate this finding, an acceptable IR speed criterion is determined by comparing the converter's RT to 90% of the inertial magnitude (pictured in Figure 5) to the average of three representative recent British nadir times. The representative nadir times include: two nadirs in 2017 both resulting from the tripping of the France-England Interconnector, $t_{Nad,31/05} = 0.12$ s and $t_{Nad,12/06} = 0.15$ s [38], and the nadir that led to significant electrical system disruption in Great Britain on the 9th of August, 2019, $t_{Nad,09/08} = 0.25$ s [39]. The resulting average nadir time that represents the critical speed that IR should be delivered before is: $t_{Nad,avg} = \mathrm{RT}_{\mathrm{acc}} = 0.173$ s. Due to the disagreement throughout industrial GFM specifications (and in academic studies) regarding "inherent and instantaneous" inertial provision, the power delivery will also be compared with the $t = 5$ ms timeframe that is often used as a threshold for instant behaviour and therefore useful inertial provision [23]–[27].

The NG ESO grid code update also included a minimum acceptable damping coefficient that GFMs could connect with: $\zeta = 0.2$ [23]. Presumably, this is defined to standardise the dynamic performance. Limiting the damping can mitigate undesired overshoot of converter components during the initiation of inertial delivery and the undershoot of nominal power during the cessation of inertial delivery—both quantified as the reduction of overshoot (OS). Furthermore, specifying the damping can limit the time that oscillations are present in the system—quantified as the reduction of settling time (ST).

Inertial devices can be considered as standard second order systems, which allow the definition of the acceptable limits of OS and ST from this minimum acceptable damping allowed by NG ESO. According to (10), the maximum OS accepted by NG ESO is $OS_{acc} = 52.7\%$.

$$OS = e^{-\frac{\zeta\pi}{\sqrt{1-\zeta^2}}} * 100. \tag{10}$$

Then, according to (11) and the range of grid voltage magnitudes $V_g$, coupling impedances $X_L$, and converter voltage angle differences $\delta$ tested throughout the study (that define the synchronising torque coefficient $K_s$ (13) and hence the natural frequency of the Swing Equation transfer function $\omega_n$ (12)), the maximum ST accepted by NG ESO is $ST_{acc} = 1.69$ s.

$$ST = -\frac{\ln\left(\alpha\sqrt{1-\zeta^2}\right)}{\zeta\omega_n}, \tag{11}$$

$$\omega_n = \sqrt{\frac{K_s\omega_0}{2HS_n}}, \tag{12}$$

$$K_s = \frac{V_c V_g}{X_L}\cos(\delta), \tag{13}$$

where $\alpha = 0.02$ is the ST tolerance and $V_c$ is the PU converter voltage magnitude. The critical features identified in the inertial criteria and the corresponding thresholds for their acceptability in response to a frequency ramp are pictured in Figure 5.

### 5.2 | Network frequency perturbation plot

The Network Frequency Perturbation (NFP) plot (example in Figure 6), which was proposed for the assessment of fre-

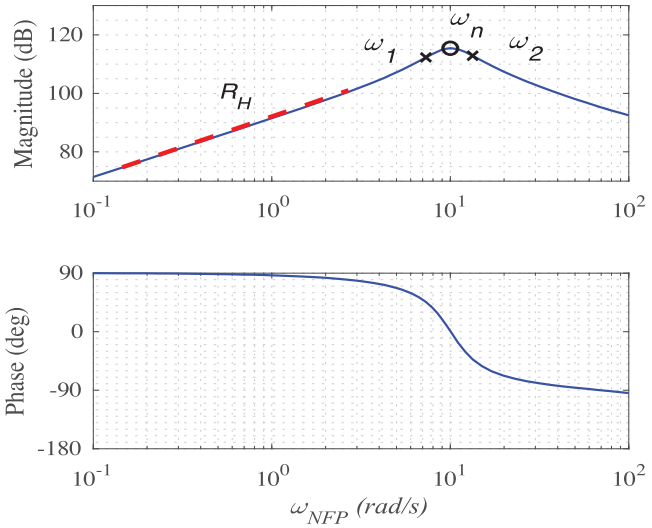


**FIGURE 6** Example Network Frequency Perturbation (NFP) plot with inertial asymptote $R_H$, natural frequency $\omega_n$, and frequency pair 3 dB below natural frequency $\omega_{1,2}$

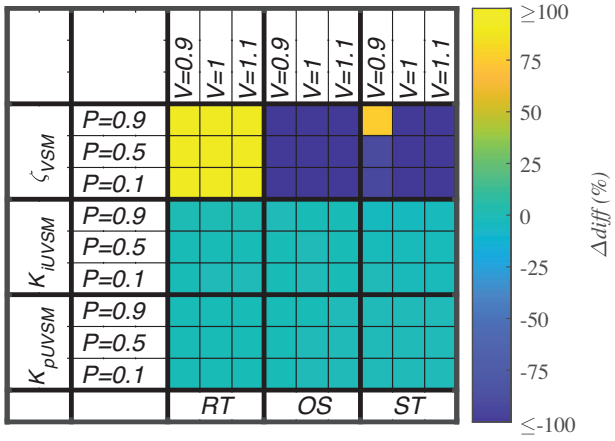


**FIGURE 7** Maximum change of time-domain properties during GFM parallel-control parametric sweeps across different operating points on SCR = 3 grid

quency supporting devices in [40], was included in NG ESO's GFM grid-code document to aid the assessment of "true" IR [23]. The NFP plot is a bode plot of a device's active power response to grid frequency disturbances. If the device provides an IR its magnitude will track an inertial asymptote $R_H$ (16) and its phase will precede the steady state phase by $90^o$, between the regions $\omega_{NFP} = 0.25$ to 13 $rad\ s^{-1}$, as defined by [40].

$$R_H\ (\omega_{NFP}) = -j2H\left(\frac{\omega_{NFP}}{\omega_0}\right), \tag{14}$$

where $\omega_{NFP}$ is the oscillation frequency of the input signal. The inertial resonant peak will occur at the natural frequency $\omega_n$ of the inertial transfer function [41], the same as that described in (14). The damping of the response can be found using classical control theory's Quality factor $Q$, by comparing this natural frequency with its two neighbouring frequencies $\omega_1$, $\omega_2$ that exist 3 db lower than the resonant peak (15).

$$Q = \frac{1}{2\zeta} = \frac{\omega_n}{\omega_2 - \omega_1}. \tag{15}$$

Finally, the phase provides useful information about the delivery of the IR. The further (to higher $\omega_{NFP}$) the device can sustain high phase (that precedes the steady-state phase by close to $90^o$) the faster and more effective the IR will be.

Although there is no suggestion that any feature of the NFP plot will be used as a specific criterion to qualify provision, it has been suggested that it can be used to help identify useful responses. Therefore, the NFP plot will be included in the assessment of different tools to differentiate between GFM and GFL IR and hence the discussion of "true" inertial features.

## 6 | RESULTS

The ability of the GFM and GFL to provide acceptable IR with respect to the representative industrial criteria identified in Section 5.1 at different power, voltage, and SCR conditions are assessed in Sections 6.1 and 6.2, respectively. Comparisons of the optimal inertial configurations for the two controllers (defined in terms of the critical features identified from Sections 6.1 and 6.2) are made in Section 6.3 on different SCR infinite bus representations of a network. The ability of each control to sustain acceptable responses across a range of inertia constants is then assessed in Section 6.4. Finally, the findings from the infinite bus simulations are validated on the multi-bus power system model and the impact that the inertial properties have on the system's frequency stability are identified in Section 6.5.

### 6.1 | Grid-forming control

The maximum change ($\Delta diff$) in the inertial time-domain properties during different parallel-control parametric sweeps are shown for the GFM in Figure 7. $\Delta diff$ is expressed as a percentage of the mean of the property during its parametric sweep and the colour indicates the magnitude and direction (during the sweep) of the maximum change (while the controller remains stable). These property-parameter interactions are further broken down according to the power (on the $y$-axis) and the voltage conditions (on the $x$-axis), while the grid strength is constant at $SCR = 3$.

The maximum changes vary depending on the parameter and property. Neither $K_{p,UVSM}$ nor $K_{i,UVSM}$ have a significant impact on any of the inertial properties. However, an increase of $\zeta_{VSM}$ increases the RT and decreases the OS and ST by more than 100 %. An outlier exists for $P = 0.9$, $V = 0.9$ due to the reduced stability range and apparent increase in ST.

Figure 8 exhibits the acceptability of the GFM inertial properties with respect to the criteria defined in Section 5.1. The

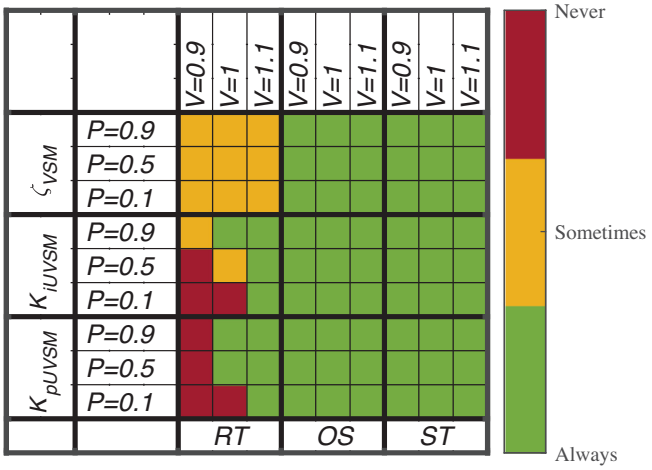


**FIGURE 8** Acceptability of time-domain properties (with respect to the criteria defined in Section 5) during GFM parallel-control parametric sweeps across different operating points on SCR = 3 grid

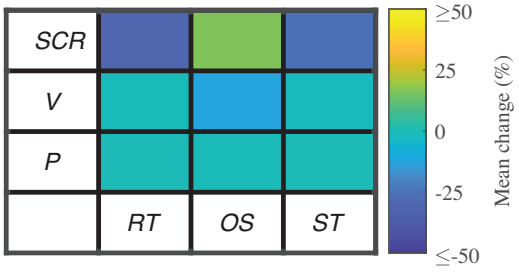


**FIGURE 9** Mean change in GFM time-domain property ranges as Power (P), Voltage (V), and SCR vary

acceptability is arranged in the same format as Figure 7, with property-parameter interactions broken down according to power and voltage conditions on the $SCR = 3$ grid. The colour indicates the ability of the GFM to meet the relevant acceptable property criterion either always (green), sometimes (amber), or never (red) during the given parametric sweep.

The GFM is always capable of meeting the OS and ST limits (for the given $SCR = 3$ grid). However, the RT limits are not always met, meaning there are some configurations on the $SCR = 3$ grid when the GFM does not qualify according to the representative industrial inertial acceptability criteria. Both voltage-controller parametric sweeps achieve acceptable RT with the base $\zeta_{VSM}$ tuning in high voltage conditions but are slowed in low voltage conditions where the parameters' low impact is unable to affect the acceptability of the RT significantly. However, the high impact of $\zeta_{VSM}$ on the RT (as shown in Figure 7) means that the GFM can be tuned to be acceptable in all of the tested conditions. The GFM requires low $\zeta_{VSM}$ to provide an acceptably fast IR in the low voltage conditions on the $SCR = 3$ grid.

Figure 9 depicts the magnitude and direction of the mean change in inertial property ranges (across all of the parallel-control parametric sweeps) as the variable operating conditions increase. For example, no significant or consistent changes are observed in any of the property values as the power level increases. This finding is consistent with Figure 8 which did not show a consistent change in acceptability as power changes.

RT experiences a small decrease as voltage increases. Despite the small magnitude of this average change (−1.1 %), the boundary acceptable GFM RT for $SCR = 3$ means that the minor decrease allows the property to become acceptable in high-voltage conditions during the voltage-control parametric sweeps, as shown in Figure 8. OS experiences a larger decrease as voltage increases.

The most significant relationship between the GFM's inertial properties and operating condition are observed for SCR. RT and ST decrease significantly (speed up) as SCR increases (grid strengthens), while OS increases. Neither OS nor ST break the relevant time-domain specifications in any grid-strength conditions, however, extreme low $\zeta_{VSM}$ settings combine with undesirable operating conditions to drive these inertial properties to approach the limits of the representative industrial inertial acceptability criteria. For low $\zeta_{VSM}$ settings, OS approaches 51 % on high SCRs and ST exceeds 1.1 s on low SCRs. On the very weak grid the GFM RT is slow, so requires a very low $\zeta_{VSM}$ to qualify as "useful" IR according to the industrial criteria, but is sped up and therefore meets the specifications across a wider range of $\zeta_{VSM}$ settings as the grid strengthens.

## 6.2 | Grid-following control

The maximum change experienced by the GFL on a $SCR = 3$ grid during each parallel-control parametric sweep is pictured in Figure 10. The GFL's IR properties all exhibit a clear and strong dependence on the inertial-filter time-constant, where its inverse is labelled $\omega_{iner}$. Each inertial property exhibits $|\Delta diff| \geq 100$ % throughout the filter time-constant sweep for all power and voltage conditions. As the filter time-constant decreases ($\omega_{iner}$ increases) the RT decreases, the OS increases, and the ST decreases. The filter time-constant also has a significant impact on the stability of the GFL. The fastest filter time-constant that ensures a stable response across all of the simulation conditions is $\tau_{iner} = 0.155$ s. Therefore, to achieve meaningful and comparable results in all conditions, this was chosen as the base setting for all of the other parallel-control parametric sweeps.

The GFL's inertial properties also show high dependence on some of the remaining parallel-control parameters. OS is shown to decrease with $K_{iPLL}$ and $K_{iU}$ (although outliers skew colour coding for low voltage conditions). $K_{iP}$ is shown to have a large impact on RT and ST, both of which decrease significantly as $K_{iP}$ increases.

The acceptability of the GFL's inertial properties with respect to the representative industrial inertial criteria detailed in Section 5.1 is pictured in Figure 11 (for $SCR = 3$). The GFL is always capable of meeting the OS and ST requirements throughout all of the parallel-control parametric sweeps on the $SCR = 3$ grid.

The GFL's RT can also be tuned to meet the acceptability criteria during the inertial-filter time-constant sweep due to

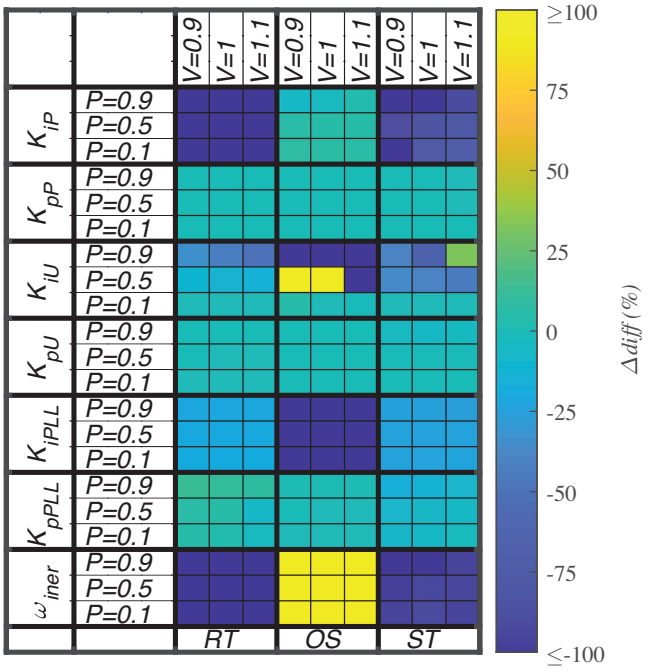


**FIGURE 10** Maximum change of time-domain properties during GFL parallel-control parametric sweeps across different operating points on SCR = 3 grid

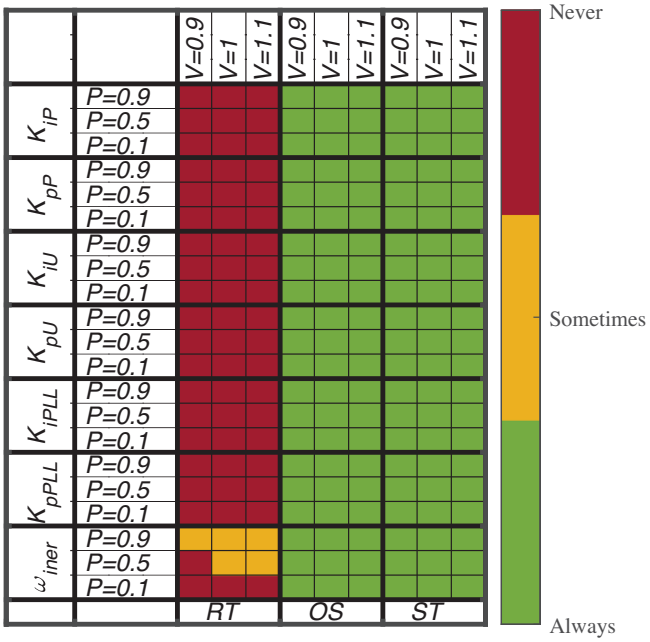


**FIGURE 11** Acceptability of time-domain properties (with respect to the criteria defined in Section 5) during GFL parallel-control parametric sweeps across different operating points on SCR = 3 grid

its large impact on the time-domain properties. However, the remaining parallel-control sweeps are never able to meet the RT specifications due to the use of the slower base setting $\tau_{iner} = 0.155$ s.

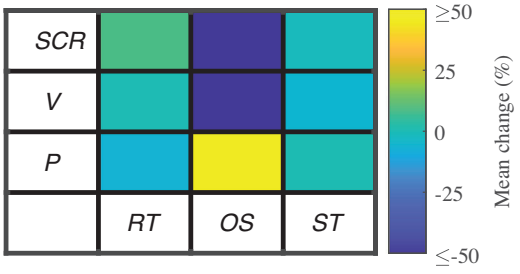


**FIGURE 12** Mean change in GFL time-domain property ranges as Power (P), Voltage (V), and SCR vary

**TABLE 3** Optimal parallel-control tuning on different grid strengths.

| | *SCR* | 1.5 | 3 | 5 |
|---|---|---|---|---|
| **GFM** | $\zeta_{VSM}$ | 0.2 | 0.4 | 0.4 |
| **GFL** | $\tau_{iner}$ (s) | 0.153 | 0.070 | 0.060 |
| | $K_{iPLL}$ | 2.0 | 99.2 | 222.1 |
| | $K_{iP}$ | 1 | 1 | 1 |
| | $K_{iU}$ | 229.8 | 2316.8 | 1577.9 |

The mean change in inertial property ranges as the operating conditions vary are pictured for the GFL in Figure 12. The average RT range increases by 9.2% for each increase in SCR, inverse to the change experienced by the GFM. ST experiences minor increases with power and SCR. The GFL's inertial OS exhibits the largest dependence on all of the operating conditions, recording mean range changes an order of magnitude larger than any recorded for the GFM. The OS increases as power increases but decreases with voltage and SCR.

## 6.3 | Optimal control settings

An optimal inertial tuning configuration for each controller is defined in Table 3 for each SCR using the findings of the sections above. An "optimal" configuration is one that minimises as many of the critical IR features detailed in the industrial specifications as possible. RT is prioritised as it is the feature that most commonly exceeds its acceptable threshold. The inertia constant is kept at $H = 2$ s. Figure 13 compares the IRs of the optimally tuned controllers and Table 4 details the response's properties relating to the inertial criteria.

The inertial properties provided by the GFL are determined by its stability. On the very weak grid the controller is less capable of supporting aggressive tuning (particularly, small inertial-filter time-constants) so the RT is slowed. Therefore, the GFL is incapable of providing acceptable IR according to the industrial criteria when $SCR = 1.5$. However, as the grid strengthens the controller stabilises, can be tuned more aggressively, and achieves fast inertial RTs.

The GFM is stable across all of the SCRs. Therefore, the GFM can be tuned aggressively to continue to meet the inertial criteria on the very weak grid, where its RT is otherwise

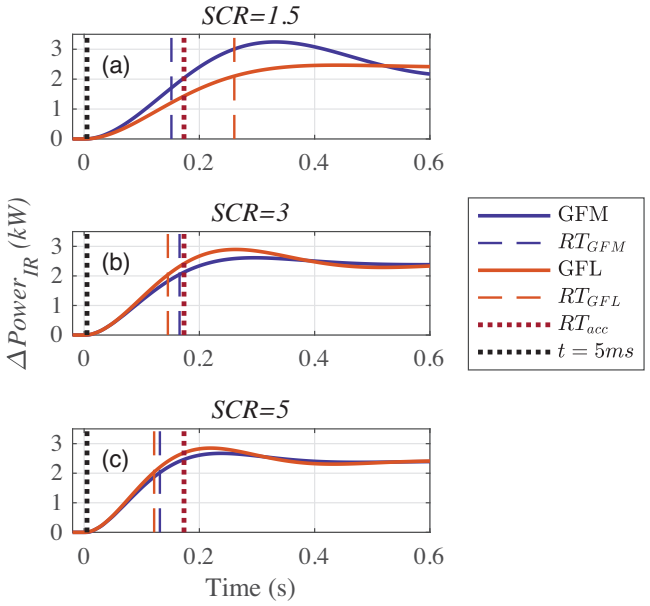


**FIGURE 13** Comparison of optimally tuned GFM and GFL controllers' inertial responses during a frequency ramp on different SCR grids for P = 0.5 and V = 1

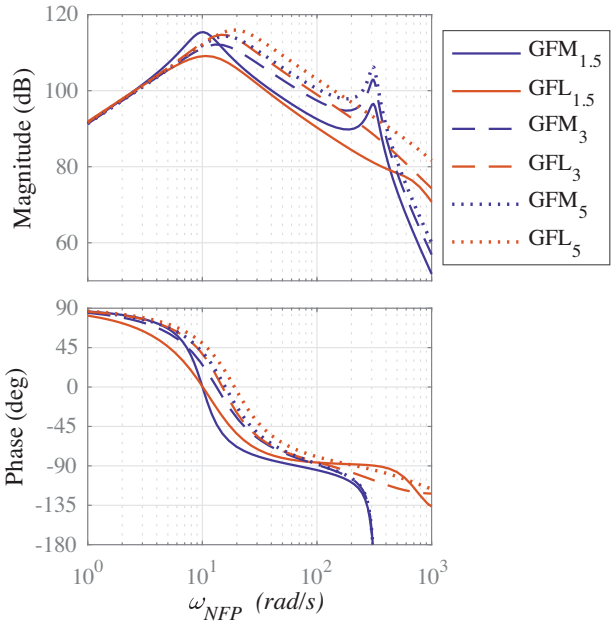


**FIGURE 14** Comparison of NFP (bode plot from grid frequency to power output) of optimally tuned GFM and GFL controllers on different SCRs (indicated by subscript)

slowed. However, this tuning results in a decrease in the GFM's damping and costs a large degradation in OS and ST. To conserve the damping and associated OS and ST, the GFM is not tuned as aggressively on grids with $SCR > 1.5$. As a result, the corresponding optimally tuned GFLs provide faster IR. Neither controller shows the ability to ramp up to any significant power output within the 5 ms period following the frequency disturbance (shown as the black dotted line in Figure 13) in any of their configurations.

Figure 14 compares the NFP plots of the optimally tuned controllers on each SCR and Table 4 includes the additional frequency-domain metrics derived from the plots. The NFP plots do not depict any clear difference between GFM and GFL IR. However, the NFP plots do help to describe the driver of the change in inertial delivery speed as SCR varies. The NFP plots show the decrease of both converter's natural frequencies $\omega_n$ as SCR decreases, which can be described by (14), (15), and the increase in the coupling impedance $X_L$. The decrease of $\omega_n$ means that on weak grids the phase is less sustained at high frequencies driving a slower response time.

**TABLE 4** Optimally tuned GFM and GFL inertial time- and frequency-domain features on different grid SCRs.

| *SCR* | 1.5 | | 3 | | 5 | |
|---|---|---|---|---|---|---|
| **Control** | **GFM** | **GFL** | **GFM** | **GFL** | **GFM** | **GFL** |
| *RT* (s) | 0.15 | 0.26 | 0.17 | 0.14 | 0.13 | 0.11 |
| *OS* (%) | 36.3 | 2.6 | 9.3 | 14.4 | 11.8 | 10.6 |
| *ST* (s) | 1.12 | 0.51 | 0.44 | 0.39 | 0.37 | 0.31 |
| $\omega_n$ (rad/s) | 10.2 | 10.6 | 12.9 | 14.6 | 16.1 | 18.2 |
| $\zeta_{app}$ | 0.32 | 0.65 | 0.64 | 0.54 | 0.57 | 0.62 |

## 6.4 | Inertial constant sweep

Parametric sweeps are carried out for both controllers to assess how wide a range of inertia constants can be supported by the tuning configurations that are deemed to be acceptable by the industrial inertia criteria. The sweeps also highlight the change in time-domain properties as the inertia varies. The GFL is tuned with an inertial-filter time-constant $\tau_{iner} = 0.1$ s, which is the lowest burden configuration that achieves an acceptable RT on the $SCR = 3$ grid. The GFM is tuned with a damping coefficient $\zeta_{VSM} = 0.4$, which is chosen as a comparable tuning as the GFL's configuration.

Figure 15 exhibits the stability of the two controllers as the inertia constant is increased. The figure is coloured to show if the controller is either: always (green), sometimes (amber), or never (red) stable for the range of tested power and voltage conditions. The GFM is always stable across all of the power and voltage conditions for all of the inertia constants. The GFL is only stable for small inertia constants and this range is reduced as the grid weakens; the maximum stable setting reduces from $H = 4$ s to $H = 2$ s as the grid weakens from $SCR = 5$ to $SCR = 1.5$.

The controllers' (stable) time-domain properties during the inertia constant sweep are pictured in Figure 16. The GFM exhibits a roughly linear increase in RT and ST and an exponential decrease in OS as H increases. The GFL exhibits a largely constant RT, a similar linear change in ST as the GFM, and an increase in OS as H increases.

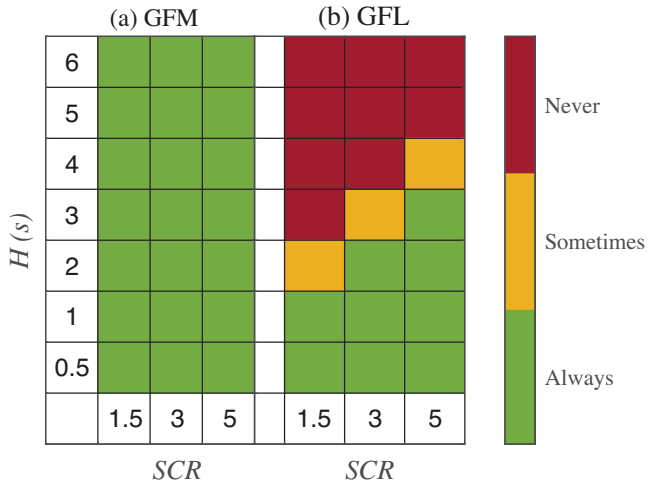


**FIGURE 15** Stability of an acceptably tuned (a) GFM and (b) GFL to support inertial constants, either always, sometimes, or never across the tested range of power and voltage grids on different SCRs

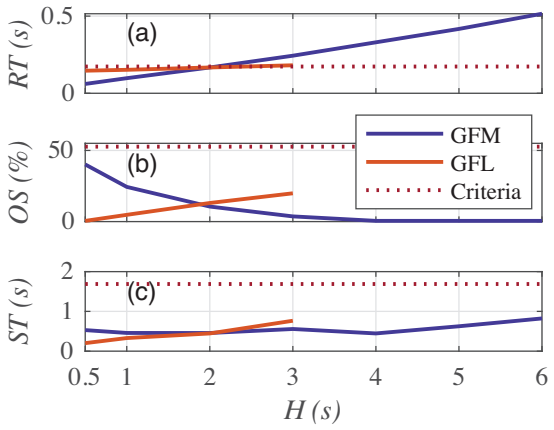


**FIGURE 16** Comparison of inertial properties (a) rise time (RT), (b) overshoot (OS), and (c) settling time (ST) during the inertial constant sweep for a GFM and GFL when P = 0.5, V = 1, and SCR = 3

### 6.5 | Validation of inertial properties and impact on system frequency

The optimal tuning configurations are implemented for both aggregated converter stations on each SCR of the adapted multi-bus power system. The impact that each controllers' configuration has on the system's ability to contain a frequency excursion in response to a load power step is assessed and the system signals are pictured in Figure 17. The figure excludes the system initialisation period from $t = 0$ to 40 s. On the weak $SCR = 1.5$ grid the less aggressively tuned GFL reaches its inertial peak ($RT = 0.15$ s) slower than the GFM ($RT = 0.10$ s) (Figure 17c). As a result, from 0.05 s to 0.3 s following the disturbance, the GFL system's ROCOF is more negative, frequency signal dips slightly lower, and SMs are required to deliver more power compared to the GFM system (Figure 17a,b,d and Table 5).

On the $SCR \geq 3$ grids, both the GFM and GFL controllers achieve similar inertial deliveries, however, both controllers' peaks are masked by a growing transient injection (Figure 17g) and k) and Table 5). The inertial peaks appear to be distinct from the faster transient injections that likely result from an angular jump, similar to the voltage-source phase response properties described in Section 2, and not from a ROCOF. Although hard to identify, the inertial peaks are measured $< 0.20$ s, which agrees with the infinite bus simulations that showed inertial $RT \geq 0.14$ s.

On the grids where $SCR \leq 3$, the minimum ROCOF is recorded for both GFM and GFL controller systems during the first 0.03 s following the disturbance (Table 5). The minimum ROCOF occurs before either controller ramps up to any significant inertial output but is more aligned with the timescales that the transient injections occur on. This suggests that, on these grids, the IR is not the critical feature that constrains the worst ROCOF. Instead, the transient injections appear to determine the critical ROCOFs. This theory is supported by the observed improvement in the minimum ROCOF as the transient injection increases (Table 5). In fact, on the $SCR = 5$ grid, both controllers' transient injections are much larger and the minimum ROCOF occurs much later, indicating a shift to a dependence on the IR to limit the (already initially better contained) ROCOF.

Irrespective of the determining feature, the GFL is shown to: 1) provide sufficiently fast IR on $SCR \geq 3$ that contains the ROCOF as well as a GFM between 0.05 s and 0.3 s following the disturbance and 2) also provide an equivalent transient injection that is as effective as the GFM at containing the ROCOF within the first instances ($< 0.05$ s) following the disturbance.

## 7 | DISCUSSION

SOs use the swing Equation (2) to describe inertial power responses to ROCOFs on the grid [9], [10], [11]. The converters' responses to pure ROCOF events on the infinite bus system clearly show that neither the GFM nor the GFL provide IR instantaneously. Specifications that expect GFMs to provide IR instantaneously (or within 5 ms) [24], [27] may have confused IR with the voltage-source transient phase response properties detailed in (1). This expectation of inertial delivery on short timescales could hinder the ability to develop and standardise system stabilising solutions.

GFL IR is conventionally disqualified from "true" status (and hence consideration for service procurement) due to the frequency measurement delay that is perceived to degrade its usefulness [23], [26]. However, the delay appears to have been observed when the GFL uses a slow averaging window-based ROCOF measurement [18]. The GFL in this paper, which uses a different Laplace-domain filtered-derivative, has been shown to be able to meet the critical delivery periods defined by the industrial criteria on grids with $SCR \geq 3$ (and even beat optimally tuned GFM alternatives). The stability, and not the delivery speed, is identified as the distinctive feature of the GFL

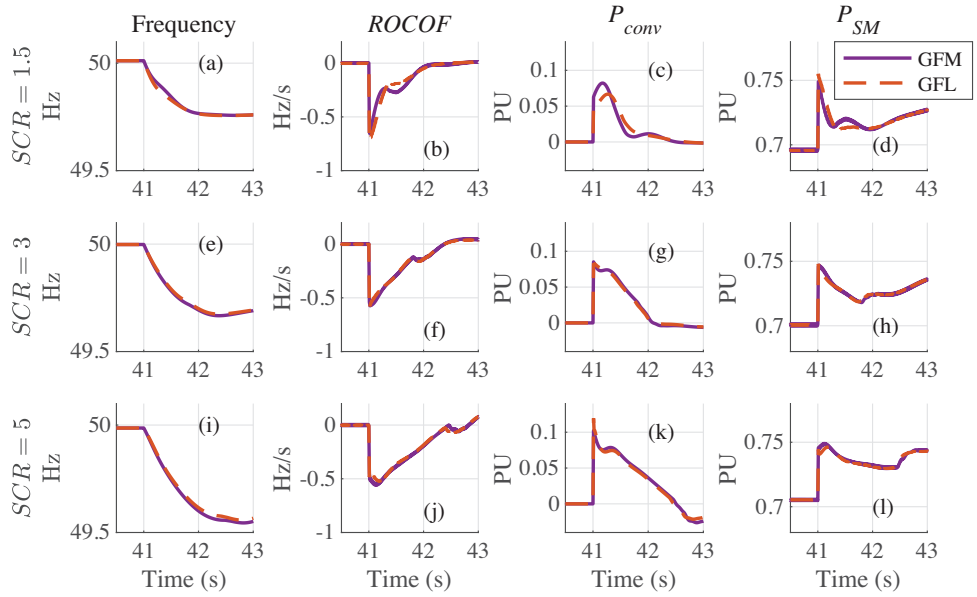


**FIGURE 17** Power system signals following a load step equal to 5% of the system's generating power capacity on different SCRs when either the optimally tuned GFM or the optimally tuned GFL provide support to the grid. Subplots (a), (e), and (i) show the frequency of a SM near the load disturbance, (b), (f), and (j) show the corresponding ROCOF, (c), (g), and (k) show the active power output by whichever converter is supporting the grid $P_{conv}$, and (d), (h), and (l) show the SM's power output $P_{SM}$

**TABLE 5** Power system features on different grid SCRs when support is provided by either the optimally tuned GFM or the optimally tuned GFL (where times features are measured since the disturbance at $t = 21$ s).

| **SCR** | **1.5** | | **3** | | **5** | |
|---|---|---|---|---|---|---|
| **Control** | **GFM** | **GFL** | **GFM** | **GFL** | **GFM** | **GFL** |
| Transient injection (PU) | 0.063 | 0.052 | 0.085 | 0.083 | 0.102 | 0.119 |
| *RT* (s) | <0.10 | 0.15 | <0.20 | <0.20 | <0.18 | <0.15 |
| Min *ROCOF* (Hz/s) | −0.657 | −0.733 | −0.574 | −0.605 | −0.559 | −0.530 |
| Min *ROCOF* time (s) | 41.02 | 41.02 | 41.03 | 41.01 | 41.14 | 41.20 |

IR, where the controller struggles to support fast inertial-filter time-constants on very weak grids. A similar range of stable GFL inertial tuning configurations was experimentally validated in [22], supporting the conclusion that fast IR can be provided from GFLs without sacrificing an acceptable level of oscillations from the frequency derivative mechanism. Advanced GFL control strategies can also be developed to mitigate their instability on weak grids [16].

The proof that these optimally tuned GFLs are equally capable at containing the grid frequency as some GFMs opposes the findings in [19], which failed to account for the full capability of the GFL, and supports the inclusion of GFLs in inertial services on stronger grids. This inclusion would increase the availability of frequency stabilising solutions and could enhance the uptake of converter-based solutions due to the increased confidence surrounding GFL's effective current limitation and the simple control adaptation. Of course, specific inertial dynamics may vary with different control (both GFM and GFL) configurations, but these results have highlighted that useful IR is not unique to GFMs.

The time-domain specifications being used by SOs to qualify IR could be used in their current state (so long as they properly reflect realistic IR timescales) as this paper has confirmed that the provision of faster IR can better contain ROCOF after the initial instances of the disturbance (and that both useful controllers can qualify according to this criterion). However, the industrial specifications may be flawed due to the intrinsic link between inertia constant, delivery speed, and nadir time. The RT criterion was integrated into this paper from the specifications to capture the critical nature of useful inertial provision before the frequency nadir [19]. It could be difficult for a SO to establish a meaningful critical delivery period to qualify new supporting devices if the critical period (nadir time) depends on the efficacy of the inertial provision from the new devices themselves.

A reliable approach needs to be developed to ensure that if the time domain criteria are used the corresponding tests and qualifying thresholds are sufficient to ensure acceptable inertial provision in all of the expected operating conditions. Equally, the time-domain property based specification encourages low damping responses to achieve the critical delivery speed criterion, which is a particular problem on weak grids where issues associated with current and voltage oscillations and interactions between devices are already a key issue [2].

The power system simulations also highlighted the importance of transient injections for the initial containment of the ROCOF, resembling the voltage-source transient phase

response described by (1). The results agree with [42] that highlighted the importance of synchronising torque and voltage-source behaviour for frequency stability and [30] that conveys the distinction of these voltage-source features from IR. An additional interesting implication is that the transient phase response may be more critical on weaker grids where the synchronising torque is reduced by the larger impedance (13).

A final complication is the apparent provision of voltage-source properties by the GFL with inertial capability exhibited by the instantaneous power injections on the multi-bus power system model. Theoretically, GFL converters are operated as current sources so should not provide power instantaneously in response to grid disturbances; however, the added inertial capability introduces a coupling between the GFL's power output and the grid angle that is thought to drive the transient phase response. This suggests that certain GFL configurations are capable of providing transient grid-stabilising injections that are also conventionally assumed to be a unique feature of GFMs.

Further work needs to be carried out to explore the ability of converters to provide voltage-source properties irrespective of their controls and to consider the impact that current limiters will have on the feasibility of their grid stabilisation, which will affect both converters (due to their equally strict thermal limits). System-wide considerations may need to be made to ensure sufficient synchronising forces related to the transient phase responses are present to stabilise the voltage angle on future converter-dominated grids. It will also be important to validate that the same transient phase phenomena are observed on experimental and real-world converter configurations, despite this exemplification of their fundamental features.

## 8 | CONCLUSIONS

This study has been developed to improve the transparency of the provision of frequency stabilising solutions from converters. The blanket disqualification of grid-following (GFL) inertial response (IR) from industrial specifications due to their perceived slow response is found to have stemmed from a combination of limited tests of GFL control configurations and the confusion of qualifying IR features with the voltage-source transient phase response. A theoretical discussion highlights the distinction between the two response types and their properties.

Parametric sweeps on an infinite bus model are used to substantiate the features of the IR and assess the ability of an example grid-forming (GFM) and GFL controller to meet the criteria used in the industry. The claim that IR is instant in some industrial specifications is proven to be wrong. The GFL is less stable than the GFM on weak grids but its IR can be tuned to meet the industrial criteria on stronger grids, including the critical delivery speed requirement.

Multi-bus power system simulations test the optimal configurations of the controllers that best meet the criteria, validating the time-domain features of the example GFM and GFL IRs on a more realistic system, and confirming that there are no hidden features of the GFM IR that better stabilises the system frequency. However, the results also highlight the importance of the transient phase response to limit the initial frequency excursion.

The results highlight that more focus should be paid to transient phase responses for system stabilisation independently from IR, particularly on weak grids. The existing industrial time-domain approach to qualify useful IR can continue to be used but needs to be updated to accurately represent inertial (and not voltage-source related transient) timescales and allow at least the consideration of GFL solutions. One flaw in the time-domain approach is the interdependence of the critical inertial delivery speed criterion and the nadir time, which needs to be considered when establishing the qualifying procedure.

Inertial response may not be the optimal approach to stabilise a converter dominated system, however, it currently appears to be necessary to support the transition towards net-zero operation while SMs continue to operate on our networks. The assessed GFL IR is not suggested to be superior to any or all GFM IRs, however, recognising that inertia is not unique to GFMs and allowing the consideration of all useful solutions could support a more effective transition, where GFMs will be needed to support the grid in many other ways.

## ACKNOWLEDGEMENTS

This work was supported by the Engineering and Physical Sciences Research Council, Grant Reference: EP/L016680/1.

## CONFLICT OF INTEREST STATEMENT

The authors declare no conflicts of interest.

## DATA AVAILABILITY STATEMENT

All of the data underpinning this publication are openly available from the University of Strathclyde KnowledgeBase at https://doi.org/10.15129/c6c137a8-ad00-48c0-8958-38527c140c8c.

## ORCID

*Sam Harrison* https://orcid.org/0000-0002-2898-4537

## REFERENCES

1. Kundur, P., Power System Stability and Control. McGraw-Hill Education, New York (1995)
2. Matevosyan, J., et al.: Grid-forming inverters: Are they the key for high renewable penetration? IEEE Power Energy Mag. 17(6), 89–98 (2019). https://doi.org/10.1109/MPE.2019.2933072
3. Edmunds, C., Martín-Martínez, S., Browell, J., Gómez-Lázaro, E., Galloway, S.: On the participation of wind energy in response and reserve markets in Great Britain and Spain. Renew. Sustain. Energy Rev. 115, 109360 (2019). https://doi.org/10.1016/j.rser.2019.109360
4. O'Sullivan, J., Rogers, A., Flynn, D., Smith, Mullane, A., O'Malley, M.: Studying the maximum instantaneous non-synchronous generation in an island system—Frequency stability challenges in Ireland. IEEE Trans. Power Syst. 29(6), 2943–2951 (2014). https://doi.org/10.1109/TPWRS.2014.2316974
5. Gu, H., Yan, R., Saha, T.K.: Minimum synchronous inertia requirement of renewable power systems. IEEE Trans. Power Syst. 33(2), 1533–1543 (2018). https://doi.org/10.1109/TPWRS.2017.2720621
6. Paolone, M., et al.: Fundamentals of power systems modelling in the presence of converter-interfaced generation. Electr. Power Syst. Res. 189, 106811 (2020). https://doi.org/10.1016/j.epsr.2020.106811

7. Beck, H.-P., Hesse, R.: Virtual synchronous machine. In: 2007 9th International Conference on Electrical Power Quality and Utilisation, pp. 1–6. IEEE, Piscataway (2007). https://doi.org/10.1109/EPQU.2007.4424220
8. Zhong, Q.-C., Weiss, G.: Synchronverters: Inverters that mimic synchronous generators. IEEE Trans. Ind. Electron. 58(4), 1259–1267 (2011). https://doi.org/10.1109/TIE.2010.2048839
9. Pogaku, N., Prodanovic, M., Green, T.C.: Modeling, analysis and testing of autonomous operation of an inverter-based microgrid. IEEE Trans. Power Electron. 22(2), 613–625 (2007). https://doi.org/10.1109/TPEL.2006.890003
10. Cvetkovic, I., Boroyevich, D., Burgos, R., Li, C., Mattavelli, P.: Modeling and control of grid-connected voltage-source converters emulating isotropic and anisotropic synchronous machines. In: 2015 IEEE 16th Workshop on Control and Modeling for Power Electronics (COMPEL), pp. 1–5. IEEE, Piscataway (2015). https://doi.org/10.1109/COMPEL.2015.7236454
11. Sinha, M., Dörfler, F., Johnson, B.B., Dhople, S.V.: Uncovering droop control laws embedded within the nonlinear dynamics of Van der Pol oscillators. IEEE Trans. Control Netw. Syst. 4(2), 347–358 (2017). https://doi.org/10.1109/TCNS.2015.2503558
12. Kryonidis, G.C., Malamaki, K.-N.D., Mauricio, J.M., Demoulias, C.S.: A new perspective on the synchronverter model. Int. J. Electr. Power Energy Syst. 140, 108072 (2022), https://doi.org/10.1016/j.ijepes.2022.108072
13. Shekhar, A., et al.: Report on laboratory tests. In: Horizon 2020, D6.2. Publications Office of the European Union, Luxembourg (2021)
14. Suvorov, A., Askarov, A., Bay, Y., Maliuta, B., Achitaev, A., Suslov, K.: Comparative small-signal stability analysis of voltage-controlled and enhanced current-controlled virtual synchronous generators under weak and stiff grid conditions. Int. J. Electr. Power Energy Syst. 147, 108891 (2023). https://doi.org/10.1016/j.ijepes.2022.108891
15. Chen, S., Zhang, X., Wu, Y., Zhu, Q., Bao, C., Zhan, X.: Segmented adaptive control of virtual inertia for virtual synchronous machines. In: 2022 7th International Conference on Power and Renewable Energy (ICPRE), pp. 176–181. IEEE, Piscataway (2022). https://doi.org/10.1109/ICPRE55555.2022.9960672
16. Wu, G., et al.: Analysis and design of vector control for VSC-HVDC connected to weak grids. CSEE J. Power Energy Syst. 3(2), 115–124 (2017). 10.17775/CSEEJPES.2017.0015
17. Morren, J., de Haan, S.W.H., Kling, W.L., Ferreira, J.A.: Wind turbines emulating inertia and supporting primary frequency control. IEEE Trans. Power Syst. 21(1), 433–434 (2006). https://doi.org/10.1109/TPWRS.2005.861956
18. Yu, M., et al.: Use of an inertia-less virtual synchronous machine within future power networks with high penetrations of converters. In: 2016 Power Systems Computation Conference (PSCC), pp. 1–7. IEEE, Piscataway (2016). https://doi.org/10.1109/PSCC.2016.7540926
19. Marchgraber, J., et al.: Comparison of control strategies to realize synthetic inertia in converters. Energies 13(13), 3491 (2020). https://doi.org/10.3390/en13133491
20. Phurailatpam, C., Rather, Z.H., Bahrani, B., Doolla, S.: Estimation of non-synchronous inertia in AC microgrids. IEEE Trans. Sustain. Energy 12(4), 1903–1914 (2021). https://doi.org/10.1109/TSTE.2021.3070678
21. Coffey, S., Morris, J.F., Egea-Alvarez, A.: Stability limits and tuning recommendation of the classical current control providing inertia support. In: 2021 IEEE Madrid PowerTech, pp. 1–6. IEEE, Piscataway (2021). https://doi.org/10.1109/PowerTech46648.2021.9495074
22. Qi, Y., Deng, H., Liu, X., Tang, Y.: Synthetic inertia control of grid-connected inverter considering the synchronization dynamics. IEEE Trans. Power Electron. 37(2), 1411–1421 (2022). https://doi.org/10.1109/TPEL.2021.3106948
23. GC0137: Minimum Specification Required for Provision of GB Grid Forming (GBGF) Capability (Formerly Virtual Synchronous Machine/VSM Capability). National Grid ESO, Workgroup Consultation (2021)
24. Application of Advanced Grid-Scale Inverters in the NEM. Australian Energy Market Operator, Melbourne (2021)
25. FNN-Guideline Grid Forming Behaviour of HVDC Systems and DC-Connected PPMs. VDE FNN, Berlin, Germany (2020)
26. Christensen, P., et al.: High Penetration of Power Electronic Interfaced Power Sources and the Potential Contribution of Grid Forming Converters. ENTSO-E Technical Group on High Penetration of Power Electronic Interfaced Power Sources (2020)
27. Kersic, M., et al.: Testing Characteristics of Grid Forming Converters Part I: Specification and Definition of Behaviour (2020)
28. Eriksson, R., Modig, N., Elkington, K.: Synthetic inertia versus fast frequency response: A definition. IET Renew. Power Gener. 12(5), 507–514 (2018). https://doi.org/10.1049/iet-rpg.2017.0370
29. Lin, Y., et al.: Research Roadmap on Grid-Forming Inverters. National Renewable Energy Laboratory, Golden, CO (2020)
30. Bakhtvar, M., Vittal, E., Zheng, K., Keane, A.: Synchronizing Torque Impacts on Rotor Speed in Power Systems. IEEE Trans. Power Syst. 32(3), 1927–1935 (2017). https://doi.org/10.1109/TPWRS.2016.2600478
31. Harrison, S., Papadopoulos, N., Silva, R.D., Kinsella, A., Gutierrez, I., Egea-Alvarez, A.: Impact of wind variation on the measurement of wind turbine inertia provision. IEEE Access 9, 122166–122179 (2021). https://doi.org/10.1109/ACCESS.2021.3109504
32. Henderson, C., Vozikis, D., Holliday, D., Bian, X., Egea-Àlvarez, A.: Assessment of grid-connected wind turbines with an inertia response by considering internal dynamics. Energies 13(5), 1038 (2020). https://doi.org/10.3390/en13051038
33. Performance of three PSS for interarea oscillations. *Mathworks*. https://uk.mathworks.com/help/sps/ug/performance-of-three-pss-for-interarea-oscillations.html. Accessed 9 May 2022
34. Abdelrahim, A., McKeever, Smailes, M., Egea-Àlvarez, A., Ahmed, K.: Modified grid forming converter controller with fault ride through capability without PLL or current loop. In: 18th International Wind Integration Workshop. Energynautics, Langen (2019)
35. Egea-Alvarez, A., Junyent-Ferre, A., Gomis-Bellmunt, O.: Active and reactive power control of grid connected distributed generation systems. In: L. Wang, E. Berlin (Eds) Modeling and Control of Sustainable Power Systems: Towards Smarter and Greener Electric Grids. Springer, Berlin Heidelberg (2012)
36. Egea-Alvarez, A., Fekriasl, S., Hassan, F., Gomis-Bellmunt, O.: Advanced vector control for voltage source converters connected to weak grids. IEEE Trans. Power Syst. 30(6), 3072–3081 (2015). https://doi.org/10.1109/TPWRS.2014.2384596
37. Harrison, S., Henderson, C., Papadopoulos, N., Egea-Alvarez, A.: Assessment of droop and VSM equivalence considering the cascaded control dynamics. In: 17th International Conference on AC and DC Power Transmission (ACDC 2021), pp. 126–131. IEEE, Piscataway (2021)
38. Roscoe, A., et al.: Practical experience of operating a grid forming wind park and its response to system events. In: 18th International Wind Integration Workshop. Energynautics, Langen (2019)
39. Technical Report on the events of 9 August 2019. ofgem. https://www.ofgem.gov.uk/sites/default/files/docs/2019/09/eso_technical_report_-_final.pdf. Accessed 2 January 2022
40. Yu, M., et al.: Instantaneous penetration level limits of non-synchronous devices in the British power system. IET Renew. Power Gener. 11(8), 1211–1217 (2017). https://doi.org/10.1049/iet-rpg.2016.0352
41. Dyśko, A., et al.: Testing characteristics of grid forming converters Part III: Inertial behaviour. In: 19th Wind Integration Workshop. Energynautics, Langen (2020)
42. Orihara, D., et al.: Contribution of voltage support function to virtual inertia control performance of inverter-based resource in frequency stability. Energies 14(14), 4220 (2021). https://doi.org/10.3390/en14144220


**How to cite this article:** Harrison, S., Henderson, C., Papadopoulos, N., Egea-Alvarez, A.: Demystifying inertial specifications; supporting the inclusion of grid-followers. IET Renew. Power Gener. 1–15 (2023). https://doi.org/10.1049/rpg2.12711

## APPENDICES

This section includes details of the relevant electrical parameters for both of the models used in this paper that. Remaining information can be found in the source materials [32], [33]. All of the models use a synchronous frequency $\omega_0 = 50$ Hz, grid impedances $R_g = 0.1/SCR\,PU$ and $L_g = 0.1/\omega_0 SCR\,PU$, and filter impedances $R_f = 0.011\,PU$, $L_{f1} = 0.1\,PU$, $L_{f2} = 0.01\,PU$, and $C_f = 0.0675\,PU$. The converter model connected to the infinite bus system has a rated power $S_n = 3\,MW$ and a rated voltage $V_g = 690$ V. The adapted two area power system model has equal magnitudes of converter and synchronous generation $S_n = 200$ MW, a rated voltage $V_g = 230$ kV, transformer ratios $r = 11.5$, constant capacitive $Q_C = 20$ MVAr, reactive $P_r = 100$ MW, and inductive $Q_L = 50$ MVAr loads, and connecting impedances $R_1 = 5 * 10^{-3}$ PU, $L_1 = 4.17 * 10^{-2}$ PU, $R_2 = 2 * 10^{-3}$ PU, and $L_2 = 1.67 * 10^{-2}$ PU.